3. PARTICIPATION IN THE COLLECTIVE USE OF THE JET FACILITIES BY THE EFDA ASSOCIATES

F. Serra (Head), M.P. Alonso, P. Belo, D. Borba, S. Chaves, R. Coelho, C. Correia, M. Correia, S. Cortes, N. Cruz, L. Cupido, B. Gonçalves, M.E. Manso, L. Meneses, F. Nabais, M.F. Nave, R.C. Pereira, V. Plyusnin, T. Ribeiro, F.Salzedas, C. Silva, C. Varandas

3.1. INTRODUCTION

The Association EURATOM/IST has proceeded with its participation in the use of the JET Facilities by the Associates, in the frame of the "European Fusion Development Agreement" (EFDA) through the "JET Operation Contract" and the "JET Implementing Agreement".

This chapter presents the main activities carried out during this year in the areas of:

- Operation;
- Scientific exploitation;
- Performance enhancements;
- Management.

3.2. OPERATION

Table 3.1 summarizes the participation of Portuguese staff in the JET Operation Team, through Secondment Agreements with the Association EURATOM/ UKAEA.

Mr. Santiago Cortes has been working in the Motional Stark Effect (MSE) Diagnostic Group. The main activities performed in 2001 were[1]:

- Calibration of the MSE system (KS9): tuning, pini switching and gas filled torus discharges;
- Improvement of the software for data processing;
- Operation of the MSE system and discharge analysis using EFIT code with MSE constraint;
- Installation of a scanning monochromator to monitor MSE channels;
- Control of the core spectroscopy group diagnostics when in shift;
- Operation of the microwave group diagnostic in the control room.

Mr. Luis Meneses has been working in the Microwave Diagnostics Group. The main activities carried out in 2001 were:

- Operation, maintenance and updating of the KG3c reflectometry diagnostic;
- Preparation of diagnostics KG3c and KG3 for the restart of the JET operation;
- Maintenance of the diagnostic KG3 as well as its data validation and data analysis by request;
- Responsible office of the KG8b – X mode correlation reflectometer;
- Improvement of the performance of the KG3c radial correlation E-mode reflectometer during campaign C4, namely by reducing the "picked" noise and by evaluating the correct offset introduced by the electronics on the signals;
- Development of a code to analyse the acquired data;
- Studies on MHD based on the results provided by the above mentioned diagnostics.

[1] Some of these activities have been carried out in the frame of Notifications for the campaign C4.

3.3. SCIENTIFIC EXPLOITATION

3.3.1. Main activities

The Portuguese participation in the scientific exploitation of the JET Facilities included the following activities:

- Participation in the campaign C4 (Table 3.2);
- Code developments and further data analysis at JET and CFN;

focusing mainly in the following areas:

- MHD studies;
- Edge physics;
- Microwave reflectometry;
- Motion Stark Effect diagnostic;
- Thomson scattering diagnostics.

3.3.2. MHD studies

3.3.2.1. Introduction

The activity in this research area has been focused in the following topics:

- Triggering of neo-classical tearing modes by mode coupling;
- Sawtooth and impurity accumulation control in JET Radiative Mantle Discharges;
- Amplitude of sawtooth pre-cursors at the onset of neo-classical tearing modes;
- Numerical simulation of sawttoth stabilization by ICRH driven fast particles for different JET scenarios;
- Influence of the position of the ICRH resonant layer over the internal kink mode stability;
- Studies on the physics of disruptions in JET plasmas.

3.3.2.2. Triggering of neo-classical tearing modes by mode coupling[2]

The mechanism for triggering the Neoclassical-Tearing Modes (NTM) around a sawtooth crash is an important problem of tokamak physics. The possibility that the sawtooth precursor, rather than the crash, may make those modes unstable has been studied. This hypothesis is suggested by JET observations, where in the majority of the JET discharges the (m=3, n=2) NTM starts before a sawtooth crash. Relying on observations and on a critique of the assumed role of the collapse phase of the (m=1, n=1) instability the physical mechanism of destabilisation of the metastable NTM to be a forced reconnection process due to electro-dynamic mode-mode coupling was considered. Two possible trigger mechanisms were studied:

- (m=3, n=2) modes destabilized by toroidal coupling with the (m=2, n=2) sawtooth precursor;
- Non-linear coupling between modes with different toroidal numbers, with the (m=1, n=1) sawtooth precursor as the driving mode.

Name	Competence	Task Force	Topic	Availability at JET
M.F. Nave	Transport and MHD	M	3	2/1 to 30/3/2001
		S1	2.1	
F. Salzedas	MHD	M	3	8/1 to 2/2/2001
F. Nabais	Fast particles modeling	M	3	2/1 to 17/2/2001
P. Belo	Magnetic diagnostics	M	4	19/2 to 16/3/2001
C. Silva	Diagnostics for edge physics	E	1.2	8/1 to 16/2/2001
			8.1	5/3 to 15/03/2001
A. Figueiredo	Radio frequency modeling	H	4.1	29/1 to 2/3/2001
L. Meneses	Microwave diagnostics	D		15 Days
T. Ribeiro	Microwave reflectometry diagnostics	D		26/2 to 23/3/2001
S. Hacquin	Microwave propagation modelling	D S1/S2		12/2 to 16/3/2001
M.P. Alonso	Thomson scattering diagnostics	D		19/2 to 16/3/2001
S. Cortes	Motional Stark effect diagnostic	D		15 Days

Table 3.2 – Portuguese participation on the JET scientific exploitation

[2] In collaboration with "Istituto di Física del Plasma", Milano, Italy.

A key aspect of the coupling hypothesis is whether certain definite relations between modes' frequencies are experimentally observed. Examination of JET data showed that usually the (m=2, n=2) precursor does not lock to the (m=3, n=2) mode. On the other hand, if the (m=4, n=3) mode which is often present at the (m=3, n=2) onset, and a smoothly monotonic toroidal plasma rotation profile, we find that the difference between the (m=4, n=3) and the (m=1, n=1) mode frequencies provide a near match to the frequency of the (m=3, n=2) mode. This result indicates the possibility of non-linear coupling between those three modes. Modeling of JET discharges shows that for perfect frequency matching conditions the triggering of the (m=3, n=2) NTM could be due to either two-mode toroidal coupling or three-mode non-linear coupling. However, the observed mode frequencies, would exclude toroidal coupling, while being consistent with the non-linear coupling.

In order to model the onset of a (m=3, n=2) NTM, the theoretical models of non-linear coupling of triplets of rotating magnetic islands[3] and toroidal coupling[4] were used. In the case of non-linear coupling, the island width W_k evolves non-linearly as:

$$\frac{dW_k}{dt} = \Gamma_k(W_k, W_{k'}, W_{k''}, \Delta\phi) \qquad (3.1)$$

Here $(k,k',k'') = (1,2,3)$ label in turn one mode of the coupled triplet and $\Delta\phi$ is a phase difference between modes. The case when the absence of coupling the unperturbed non-linear growth rate

$$\Gamma_k^{(0)}(W < W_{thr}) \le 0$$

is considered. A perturbation due to mode coupling will add to

$$\Gamma_k^{(0)}(W_k)$$

and if sufficiently large will result in a global positive

$$\Gamma_k(W_k, W_{k'}, W_{k''}) = \Gamma_k^{(0)}(W_k) + \Gamma_{coupl}(W_k, W_{k'}, W_{k''}, \cos\Delta\phi) > 0 \qquad (3.2)$$

The unperturbed non-linear rate of growth of the k-labeled mode was taken as:

$$\Gamma_k^{(0)}(W_k) = \frac{r_s^2}{\tau_{R,k}}\{-|\Delta'_{0k}| + \beta_\theta[\frac{a_b W_k}{W_k^2 + W_d^2} - \frac{a_{pol_p}}{W_k^3 + W_{p0}^3}] + Re(\Delta'_{wall_k})\} \qquad (3.3)$$

The first term is the usual tearing mode Rutherford approximation, while the second term is the neo-classical one. The basic principle of triggering of metastable NTMs by mode coupling is illustrated in Figure 3.1, where the growth rate dW/dt dependence on W is shown for both the $\chi_\perp/\chi_{//}$ and polarization current models, with and without coupling effects and with $\beta_\theta > \beta_{\theta,crit}$ so that the mode is metastable. In the absence of mode coupling effects, the $\chi_\perp/\chi_{//}$ and polarization current models yield threshold island widths given by

$$W_{thr}^{(1)} \text{ and } W_{thr}^{(2)},$$

respectively, with

$$W_{thr}^{(2)} > W_{thr}^{(1)}.$$

When mode-coupling effects are present, the mode starts to grow at a faster pace if the polarization current effects vanish (black dashed curve). If the effect of mode coupling is weak, small saturated states result (black dot-dashed trace for the $\chi_\perp/\chi_{//}$ model). For sufficiently strong coupling effects, for both cases, at a given stage the island width may overcome either

$$W_{thr}^{(1)} \text{ or } W_{thr}^{(2)},$$

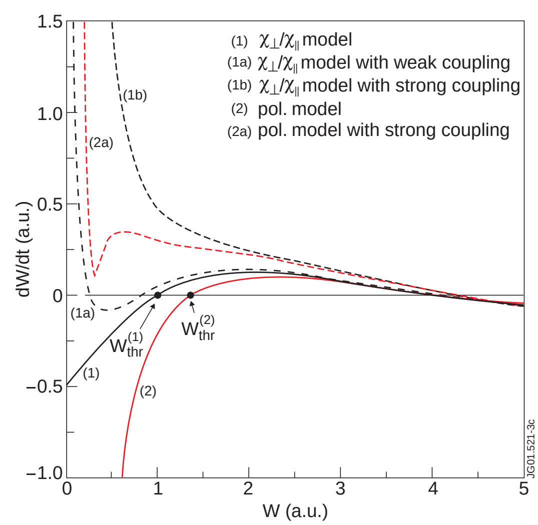

Figure 3.1 - Illustration of the principle of destabilisation of NTMs driven by mode coupling

---

[3,5] Annual Report 2000

making *irreversible* the transition to the large saturated states ($W \approx 4$, in the a.u. used in figure). Here, irreversibility means that even if the mode coupling interaction vanishes, the driven mode will still continue to grow.

3.3.2.3. Sawtooth and impurity accumulation control in JET radiative mantle discharges

Experiments have been performed at JET to test in a large machine a very successful technique used in medium-size tokamaks[5] to improve the level of confinement in high-density regimes. This technique consists on the creation of a cool radiative mantle around the plasma by injection of high-Z impurities.

The work described in this section aims to understand the loss of confinement and to consider appropriate experimental measures to improve the stationarity of ELMy H-mode discharges with high radiation fractions ($\gamma=P_{rad}/P_{tot}>0.7$) from Argon (Ar) injection. Discharges obtained in the septum configuration[6] were considered. This configuration was used to be as close as possible to the limiter Radiative Improved (RI) modes of TEXTOR. As in TEXTOR, JET experiments show that higher densities can be achieved in discharges with increased radiation level, when compared with discharges without impurity injection. However, unlike TEXTOR where large improvement in confinement is observed, impurity injection at JET does not show an improvement in overall confinement with respect to discharges without impurity. With large impurity concentrations, a sudden loss of confinement is observed.

In the JET septum configuration, the highest performance plasmas ($H_{97}*f_{GWD} \geq 0.8$) were obtained with two gas injection phases: an initial phase of continuous D_2 and Ar fuelling, followed by the "after-puff" phase when both gases injection rates are reduced. In discharges with low or moderate Ar seeding, a quasi-steady state regime remains through to the end of the applied heating. However, at high Ar injection rates ($\geq 8x10^{21}$ el/s), the high confinement phase is transient.

The degradation in confinement was found to coincide with impurity profile peaking following the cessation of sawtooth crashes[7]. Equilibrium reconstruction with the EFIT code shows typical q(0) values of ~0.9 in the puff phase. Once the gas rate is decreased, q(0) increases and sawtooth suppression occurs when q(0) rises above unity. This is mainly due to an increase in edge pedestal temperature in the after puff phase. Thus the resistivity in the plasma edge decreases and as a result the plasma current is re-distributed leading to a lower plasma current density in the plasma centre.

At JET the magnetic equilibrium reconstruction as well as MHD mode analysis indicates that near the time of sawtooth suppression the central q-profile is nearly flat and close to unity. After sawtooth suppression, equilibrium reconstruction with polarimetric measurements indicates reversed shear q-profiles. The evolution of the central q(0) into reversed shear, not observed in reference discharges without impurity, is a result of impurity accumulation. As the central q becomes non-monotonic and above unity, (m=4, n=3) and (m=3, n=2) modes may become unstable. The latter are observed to limit core density. The observation that sawtooth-free periods coincide with core impurity accumulation is similar to observations in other tokamaks[8] The effect that sawteeth and other MHD instabilities have on the impurity density profiles has been studied in detail from SXR data. It was found that in the after-puff phase both sawtooth crashes and continuous core MHD modes flattened the impurity density. It was concluded that sawteeth in these discharges play an important role in preventing impurity peaking.

Based on the results of the data analysis, experiments were designed to improve the stationarity of q(0) and consequently to maintain sawteeth. To keep q(0) below unity, a small amount of ICRF power (1-3MW) was added to the main NBI heating. The RF heating resonance layer was located on axis to increase the central electron temperature. Low ICRH power was used in order not to create a significant population of ICRH accelerated ions, thus avoiding sawtooth stabilisation by fast particles. Hydrogen was used as the minority species, with the antennas operated either in dipole, or with $-\pi/2$ phasing. In both configurations the central T_e was increased ($\Delta T_e(0) \sim 0.5$ keV), preventing q(0) increasing as fast as in the reference discharges. In these experiments, sawteeth were maintained and core impurity

[5] TEXTOR and DIII-D

[6] With the X-point embedded in the dome of the JET MKIIGB divertor.

[7] Annual report 2000

[8] Such as TEXTOR and ASDEX-Upgrade

accumulation was not observed (Figure 3.2). Loss of confinement and density was not observed. With added ICRH the high performance phase was extended and lasted in a quasi-steady state until the heating was turned off. Values of H_{97}*f_{GWD}~0.8, previously only lasting <1 τ_E at high Ar injection rates, were maintained for the duration of the heating (Δt~9τ_E).

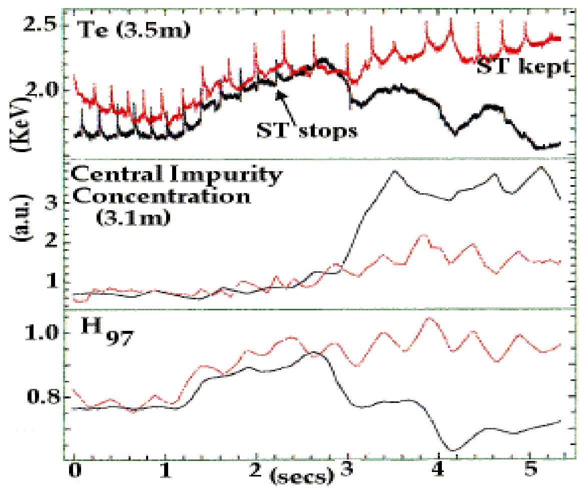

Figure 3.2 - Comparison of discharges with high Argon concentrations. In the reference discharge (P_{NBI}=12 MW), sawtooth stops, impurity peaking and loss of energy confinement are observed (black traces). In the discharge with added ICRH (P_{NBI}=12 MW plus P_{ICRH}=2 MW), the sawtooth was maintained, core impurity accumulation was prevented and, the high confinement phase was extended (red traces).

3.3.2.4. Amplitude of sawtooth pre-cursors at the onset of neo-classical tearing modes

Most observations of Neo-classical Tearing Modes (NTM) in JET experiments occur in regimes where sawteeth are present. A clear correlation between the time of sawtooth crashes and the onset of NTMs was previously obtained from a small database of pre 2000 JET experiments. The present work considers a larger database including 2000-2001 NTM studies, related with experiments for the study of shape effects on the NTM trigger, NTM studies in ASDEX-Upgrade similarity discharges, ITER like discharges and experiments to control NTMs by sawtooth control.

The main aim of this study was to find out if the NTM onset were correlated with sawtooth MHD precursor oscillations, trying to give experimental support to the idea that the NTM becomes unstable by mode-coupling interaction with the sawtooth precursor modes. The correlation between sawteeth crashes, sawteeth precursors and other central n=1 MHD modes such as fishbones and the onset of the *m*=3, *n*=2 NTMs was studied. In addition the amplitude of the n=1 sawtooth precursors around the time the NTM starts was analysed.

In the majority of cases, the NTM onset occurs before or around a sawtooth crash (Figure 3.3). Most are triggered in the presence of central n=1 modes (and their n=2 harmonics). The peak around the sawtooth crash corresponds mostly to pulses with low β_N, and very long sawtooth periods with short precursor observed in regimes with ICRH. The amplitude of *m*=1, *n*=1 modes was obtained from observations of magnetic field perturbations induced on magnetic pickup coils using fast Fourier transforms and filter techniques. The acquisition frequency of these coils varies from 250 kHz to 1 MHz. The two sawtooth crashes that were nearest to the *m*=3, *n*=2 NTM onset were considered. The sawtooth period was obtained from Soft X-ray emission traces. The mode amplitude of the sawtooth precursor nearest to NTM onset, increased with increasing β_N. The scaling of the amplitude versus β_N was qualitatively similar to the scaling of sawteeth in general.

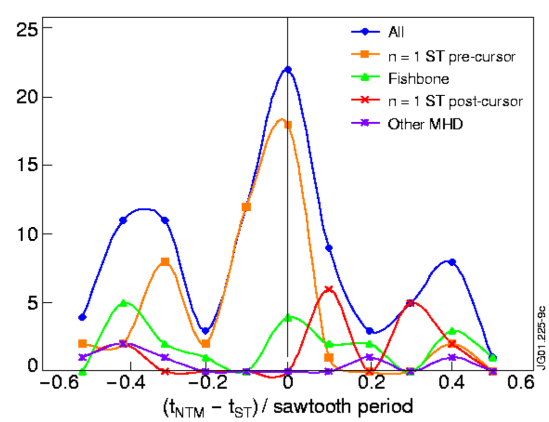

Figure 3.3 - Distribution of NTM occurrence (89 discharges) with respect to the nearest sawtooth crash (dark blue). Distribution of cases occurring when a sawtooth precursor is observed (orange, when fishbones are present (green) and with respect to n=1 sawtooth post-cursors (red).

In a minority of the discharges studied the NTM onset occurred around the maximum amplitude of a fishbone burst (Figure 3.4). The NTM was plausibly triggered by the fishbone instability. The fishbone amplitude at the (3,2) onset time had the same order of magnitude as the amplitude of the nearest *n*=1 sawtooth precursor, for similar values of β_N. Thus the required n=1 amplitude for the NTM onset appeared to be independent of whether the NTM was triggered by fishbones or sawteeth. The n=1 fishbone amplitude was observed to be in phase with the amplitude of the NTM (Figure 3.4). This suggested that the fishbone and the NTM modes were coupled. In dominantly NBI heated discharges, the onset of NTMs associated with sawteeth occurred for $\beta_N > 1.5$, while NTMs related to fishbones where observed at higher beta values, $\beta_N > 2.5$. Other factors, which govern the resistive tearing, needed to form the seed island, such as the relative rotation between q=1 and q=3/2, need to be examined in future studies. In addition, the amplitudes of higher frequency modes (with n≥3), that are important for non-linear coupling need to be investigated.

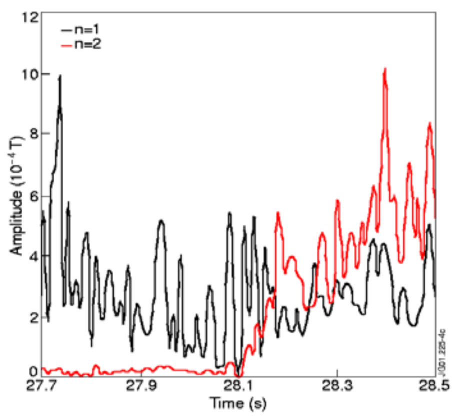

Figure 3.4 - Amplitude of the n=1 fishbone bursts and n=2 NTM modes for the shot #52083

3.3.2.5. Numerical simulation of sawtooth stabilisation by ICRH driven fast particles for different JET scenarios

The effect of the ICRH driven fast particles over the sawtooth was numerically analysed for different JET scenarios (with different NBI power) using the CASTOR-K code. The scenarios analysed were the scenario where ICRH was the only auxiliary heating method used, the scenario where a moderate NBI power (8 MW) was used along with ICRH, and the scenario where a high NBI power (20 MW) was used. The NBI unlike the ICRH can accelerate particles not only in the perpendicular direction but also in the parallel direction, inducing a plasma rotation. Since the sawteeth observed frequency depends on the plasma rotation, the effect of the ICRH driven fast particles over the internal kink mode depends on the NBI power used.

The CASTOR-K code calculates the transference of energy between the fast particles and the mode, allowing to determinate the variation on the growth rate of the mode caused by the presence of the fast particles (γ_{HOT}). The influence of the fast particles over the growth rate of the mode (γ_{HOT}) depends naturally on the fast particles population characteristics. The distribution function of fast particles used by CASTOR-K is a function of $\lambda=\mu B_0/E$, the fast ions temperature T_{HOT} and the toroidal canonical momentum P_Φ. For ICRH driven fast particles λ is the ratio between the radius of the cyclotronic resonance heating layer and the major radius.

CASTOR-K was used to calculate γ_{HOT} for a vast range of the fast particles parameters (T_{HOT} and λ which depend on the RF power and frequency respectively) and for each of the three scenarios. The results were presented under the form of contour plots (lines for identical values of γ_{HOT}). With these mappings it is possible to estimate the influence of a given ICRH driven fast particles population over an internal kink mode.

Figure 3.5 shows the mappings of the stabilising-destabilising regions for the three scenarios (ICRH-only, moderate NBI power and high NBI power). While for low frequencies of the internal kink mode, only fast ions populations characterized simultaneously by low values of T_{HOT} and λ are destabilising, for high frequencies of the mode these same populations are stabilising. High frequency internal kink modes are destabilised by populations of low values of T_{HOT} or low values of λ, but not simultaneously. For average frequencies of the mode, the destabilising region is greatly increased, including both types of populations mentioned before.

3.3.2.6. Influence of the position of the ICRH resonant layer over the internal kink mode stability

The plasma rotation with ICRH has been studied in JET experiments by varying the toroidal magnetic field throughout the heating phase. Consequently the ICRH resonance position, which depends on the magnetic field, was also varied throughout the heating phase. The influence of the position of the cyclotronic resonance on the internal kink stability was analysed with the CASTOR-K code for the discharge 51661.

The toroidal magnetic field was increased during the heating phase, while the other parameters remained approximately constant (Figure 3.6). The plasma density and the RF power were maintained constant while the safety factor on the axis increased slightly from 0.83 to 0.88. In the beginning of the heating phase, when the magnetic field was low (B_0 between 2.3 and 2.5 T) and the resonance layer was well in the high field side just outside the q=1 surface, sawtooth exhibited its usual behaviour with short sawtooth period. In this time interval, the linear normal growth rate calculated by the MISHKA code normalized to the Alfven frequency was γ= 0.0068 while the ICRH driven fast particles had a very strong destabilising effect, γ_{HOT}= 0.07. Later in the discharge, when the cyclotronic resonant layer was on the high field side, but close to the axis ($\lambda \approx$ 0.94 to 0.97), the called monster sawteeth appeared. By this time the ICRH driven fast particles had a stabilising effect, ranging from γ_{HOT}= -0.008 to γ_{HOT}= -0.024, stronger than the ideal growth rate calculated by MISHKA, γ= 0.0075. Just before the cyclotronic resonant layer reached the axis, a major sawtooth crash occurred triggering other modes and ending the sawtooth regime. Just before this crash, the ICRH driven fast particles had a weak effect, γ_{HOT}= -0.0002, not enough to compensate the internal kink growth rate, γ= 0.0075.

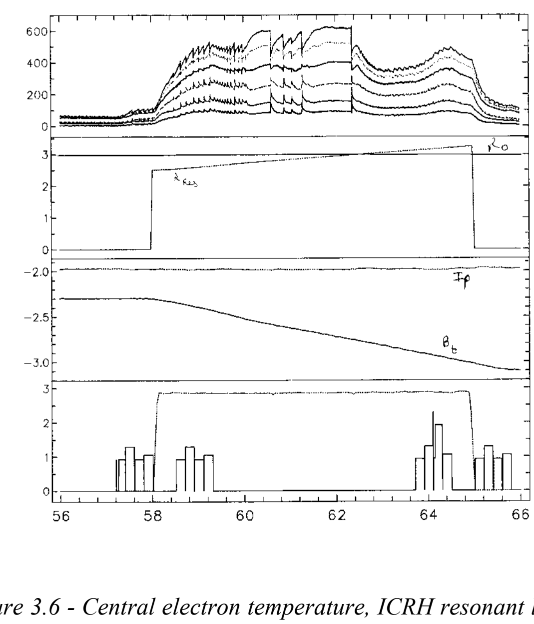

Figure 3.6 - Central electron temperature, ICRH resonant layer radius, toroidal magnetic field and ICRH and NBI power for discharge 51661.

3.3.2.7. Studies on the physics of disruptions in JET plasmas

IST/CFN has started in 2001 its participation in the understanding of the physics of disruptions in the JET plasmas, by studying the behaviour of the plasma density and electron temperature evolution during the energy quench. Direct measurements of the n_e and T_e profiles are possible with LIDAR and the ECE heterodyne radiometer. However, some improvements in the diagnostics hardware as well as in the Central Acquisition and Trigger System (CATS) are needed to achieve the adequate spatial and temporal resolutions.

During campaign C4 an IDL code was developed with a GUI interface that allows the joint display of three electron temperature signals, the slow and fast sampled ECE signals and LIDAR Te profiles. ECE signals can be displayed either in a isothermal surface of $T_e(r, t)$, or in profiles $T_e(t)$, or $T_e(r)$, the last ones together with LIDAR Te profiles. Either the displayed time window or the entire discharge can be saved to a file in IDL data format. This option is particularly useful for on-site data analysis of CATS data (since it can take a long time to load CATS data) or remote data analysis.

3.3.3. Edge physics

3.3.3.1. Introduction

The activities in this research area have been focused in the following topics:

- Fluctuations measurements using single Langmuir probe characteristics;
- Temperature fluctuations measurements using a modified triple probe;
- Comparative studies of turbulence and ExB sheared flows in He and D plasmas;
- Dynamical interplay between gradients, radial electric field and transport in JET tokamaks;
- Empirical similarity in turbulent fluxes and radial scale of turbulent transport in the JET plasma boundary region;
- Velocity fluctuations and transport in the JET boundary region.

3.3.3.2. Fluctuations measurements using single Langmuir probe characteristics

The aim of this work is to obtain information on density (n), electron temperature (T_e) and floating potential ($\widetilde{V}_f$) and their cross-correlations from single Langmuir probes characteristics. The method consists of fitting the experimentally determined probe current fluctuation level to a theoretical curve as a function of the bias; the required fluctuation levels are the coefficients, which are returned by the curve-fitting routine.

Measurements have shown that the curve fitting technique is able to resolve plasma fluctuations using single probe characteristics (Figure 3.7). This method has been applied to JET reciprocating probe data and results show that temperature fluctuations are, in general, reasonably low. In L-mode plasmas we found that close to the separatrix

$$\widetilde{T}_e / T_e \leq 0.5\,\widetilde{n}/n \cong 5\,\% \text{ and } \widetilde{V}_f / T_e \cong 25\,\%$$

which is in good agreement with results obtained from probes measuring floating potential and ion saturation current. The correlation between density and temperature, γ_{nT}, is in general high (>0.4) and γ_{TV} negative, (<-0.2). Results tend to support the standard estimation of cross-field particle flux which ignores temperature fluctuations. Therefore, temperature fluctuations do not appear to be responsible for the large cross-field particle flux measured in the JET edge plasma.

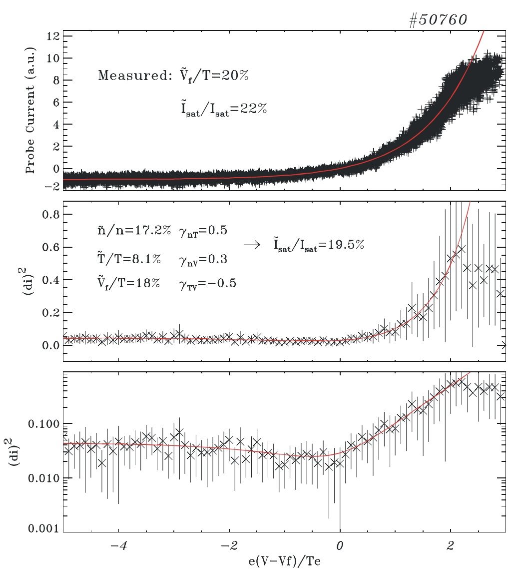

Figure 3.7 - Example of the application of the probe fluctuations analysis and derived fluctuations levels.

3.3.3.3. Temperature fluctuations measurements using a modified triple probe

The aim of this study is to evaluate the importance of the temperature fluctuation on the ExB turbulent transport. Temperature fluctuations with the appropriate phase can modify the derived particle flux from Langmuir probe measurements, being a possible explanation for the large values of the, ExB turbulent transport measurements in divertor discharges.

The new fluctuation probe head consists of modified triple probes. Five pins are used in order to cancel the fluctuations phase shift between the three pins of a standard triple probe. The effective size of the probe is 5 mm, which is smaller than the typical poloidal correlation length of fluctuation (5-10 mm).

The new fluctuations probe head has been used to measure turbulent fluxes and to test the probe design. Although some valid data were obtained, at the end of the session tips were found to be short-circuited. Deposition of carbon on the insulating material in between and around the pins was found to be the cause of that problem. We concluded therefore that the tips are too close together and that it is not possible to avoid the deposition of carbon in between the tips in the present design.

Although no temperature fluctuations measurements were made, results indicated that ion orbit effects do not appear to invalidate measurement. This was not clear since the distance between pins, 0.25 mm, is smaller than the ion Larmor radius.

3.3.3.4. Comparative studies of turbulence and ExB sheared flows in He and D plasmas

This comparative study will help to understand the role of atomic physics as a driving mechanism of turbulent transport and as a momentum sink (i.e. charge exchange mechanisms). Measurements of fluctuations, ExB sheared flows and turbulent transport in He and D plasmas were performed during the C4 campaign. Detailed analysis of the results is underway.

The scaling of the turbulent flux and diffusion coefficient with the input power, density and magnetic field has also been investigated. Different scaling properties of transport in the edge and SOL were found. Transport in the SOL does not depend on the magnetic field, contrary to the observed in the SOL, were the turbulent flux is observed to decrease with increasing B (Fig. 3.8). The effective diffusivity is in the range 1m^2/s, which is close Bohm.

The turbulent transport was also found to depend strongly on the average plasma density. The diffusion coefficient and the turbulent flux increase as the density increase, both in the SOL and the edge plasmas. In opposition, a weak dependence of the turbulent transport on the input power has been found.

A new reciprocating probe head is being developed in order to measure temperature fluctuations. The distance between pins has been increased considerably and their distribution and geometry modified to prevent the deposition of carbon. Although the size of the probe has been increased, the probe still very compact so that plasma parameters can be measured in a distance smaller than the typical poloidal correlation length of fluctuation (5-10 mm). Detailed measurements of the turbulent transport using this new probe head are planned for the C5-7 campaigns.

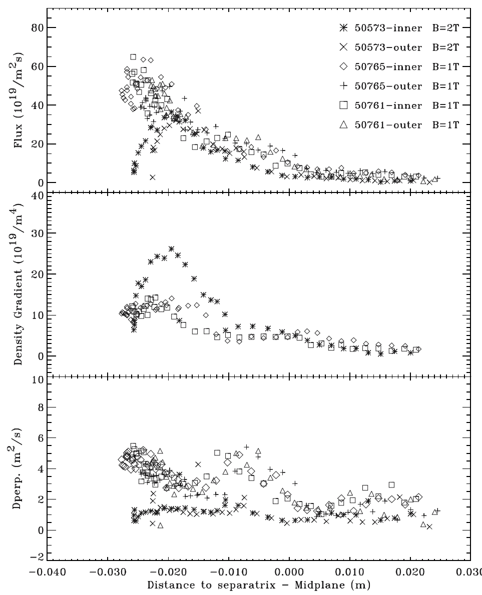

Figure 3.8 - Properties of turbulent transport scaling with magnetic field in the EDGE and SOL regions

3.3.3.5. Dynamical interplay between gradients, radial electric field and transport in JET tokamak

Conditional statistical analysis was used to obtain the density local gradient, radial electric field and turbulent flux dynamical relation from Langmuir probe signals. Results show that these parameters are correlated. The most probable value of density local gradient corresponds to a minimum of turbulent flux. Most of the flux occurs when the plasma deviates from it average gradient. Self-regulated transport through fluctuations could explain these results. The system relaxes to the most probable state in a time comparable to the decorrelation time of turbulence. L and H-mode scrape-off layer discharges where studied. The expected value of the flux for a given density gradient ($E[\Gamma_{ExB} \mid \nabla_r I_S]$) has been calculated (Figure 3.9). The expected value can be understood as the average amplitude of the flux pulses at a given gradient. For the L-mode case the density gradient probability distribution function is rather gaussian around it average gradient. The results show that most of the time the plasma is on it average gradient and the size of transport events have minimum amplitude ($\Gamma/<\Gamma>\approx 0.5$). Most of the turbulent flux occurs when the plasma displaces from it average value and large amplitude transport events ($\Gamma/<\Gamma>\approx 3$) are expected. On the H-mode case is possible to see that the PDF of gradients is less gaussian and the most probable value is below the average gradient. The amount of events with gradient above the average increases. Large amplitude transport events are expected for smaller gradients, however, around the average gradient, small amplitude flux events are expected and the transport still exhibits a minimum.

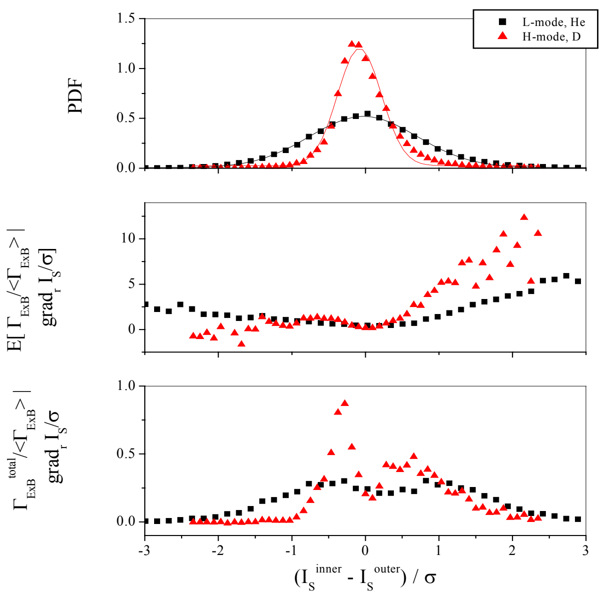

Figure 3.9a) - The probability distribution function of gradient for L-mode and H-mode discharge. For L-mode the distribution is rather gaussian. For H-mode the most probable value is below the average value; b) Expected turbulent flux at a given density gradient. The most probable value of density gradient minimizes flux events amplitude; c) Most of the transport occurs when the plasma leaves the most probable value.

The increase in the size of transport events as gradient increases is consistent with different transport mechanisms expectations (i.e. diffusive models, critical gradients) and would reflect the influence of an increase in the free energy source on transport. However, on the basis of pure diffusion type transport mechanisms, it is difficult to explain the increase in the amplitude of transport events as gradient decreases. On the context of transport self-regulated by fluctuations this increase might reflect the modification in the dynamical ExB sheared flows as the free energy source of fluctuations (gradient) decreases.

The same method was applied introducing also the radial electric field. Figure 3.10 shows that the expected value of ExB flux for a given gradient and radial electric field, $E[\Gamma_{ExB} \mid \nabla_r I_S, E_r]$, has a minimum that displays a linear relation between gradient and E_r. The contour plot shows that the combined probability density function between gradient and radial electric field is asymmetric, showing a clear dependence with radial electric field. Large amplitude transport event happens when the plasma leaves the most probable gradient. Note that the previous figure is the averaged projection of this distribution on the gradients axes. Figure 3.11 represents the expected value of displacement on the gradients, E_r space in 2 μs time interval. It shows that the plasma, on average, minimizes the amplitude flux events in a time scale comparable to the time scale of turbulence (5-10 μs). Fast relaxation is observed for bigger displacements from the average gradient. Maximum transport occurs, as before, when the plasma leaves the most probable (stable?) gradient (Figure 3.12).

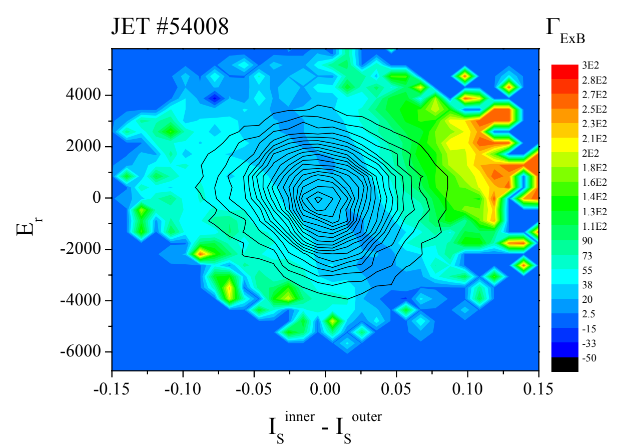

Figure 3.10 - Turbulent flux expected value for a given density gradient and radial electric field (on colour). Contour plot represents the PDF of density gradient and radial electric field distribution. The most probable value of this distribution minimizes the amplitude of turbulent flux events.

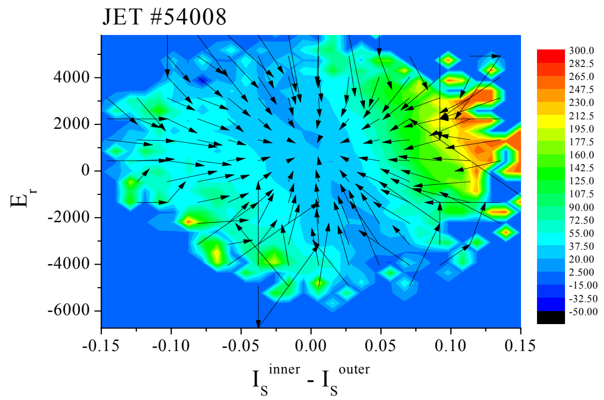

Figure 3.11 - Turbulent flux expected value for a given density gradient and radial electric field (on color). The arrow indicates the expected transition in 2 μs time interval showing that on average the plasma always returns to the most probable value (which minimizes flux events).

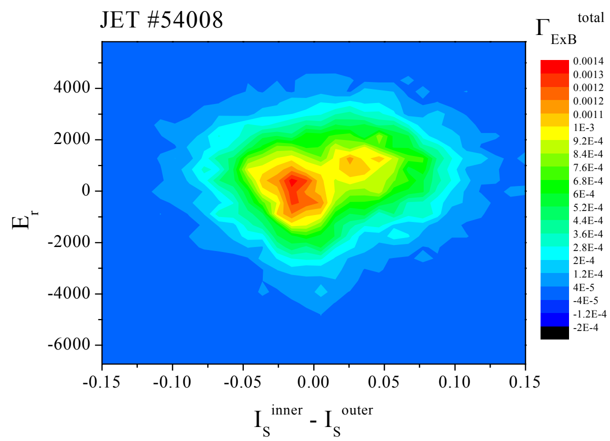

Figure 3.12 - The graphic represents the total flux that occur at a given density gradient and radial electric field. Most of the flux occurs when the plasma leaves the most probable state.

3.3.3.6. Empirical similarity in turbulent fluxes and radial scale of turbulent transport in the JET plasma boundary region

Experimental evidence of an empirical similarity in the statistical properties of turbulent transport and non-gaussian features in the radial coherence of ExB transport in the JET plasma boundary region was found just inside the separatrix.

Figure 3.13 shows the probability density function (PDFs) of the ExB turbulent fluxes for measurements taken in the plasma edge region $r - r_{sep} \approx -(1\text{-}2)$ cm. In JET, as well as in other devices, the PDFs of fluctuating transport have significant non-gaussian features. A significant fraction of the total ExB flux can be attributed to the presence of large and sporadic transport bursts, the magnitude of which are quite sensitive to the plasma conditions.

The PDF´s have an interesting property: they can be re-scaled assuming a functional form $PDF(\Gamma_{ExB}) = L^{-1}\, g(\Gamma_{ExB}/L)$ where L is a scaling factor. As shown in Figure 3.13 the re-scaled PDF´s of Γ_{ExB} show the same behavior over the entire amplitude range of transport. The scaling factor L is directly related with the level of fluctuations computed as the rms value of the ion saturation current fluctuations (Figure 3.14) and with the mean turbulent flux.

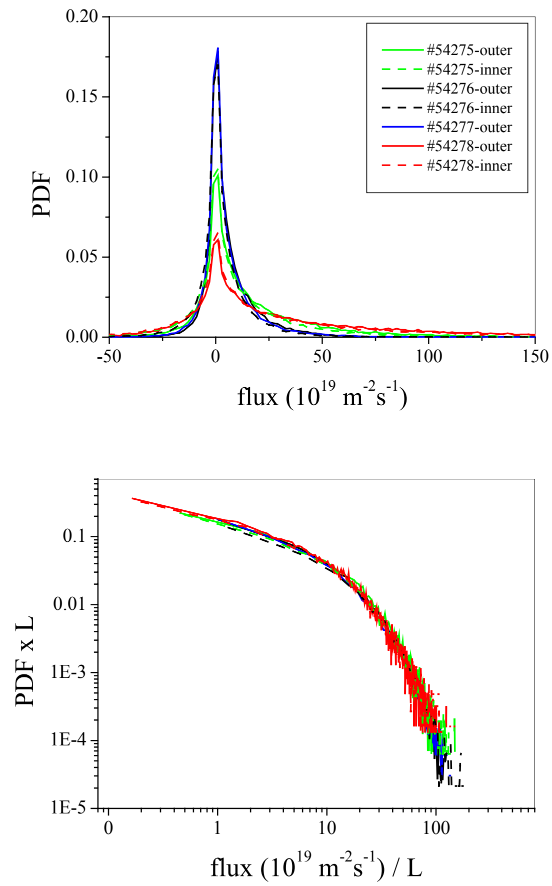

Figure 3.13 - Probability distribution function of ExB turbulent fluxes for different plasma densities measured in the plasma edge region and re-scaled PDF's.

These findings are in agreement with the empirical similarity in the frequency spectra of fluctuations reported in different fusion plasmas. This striking similarity of the PDF´s of turbulent fluxes supports the idea that plasma turbulence displays universality and provides a critical test for plasma turbulence models.

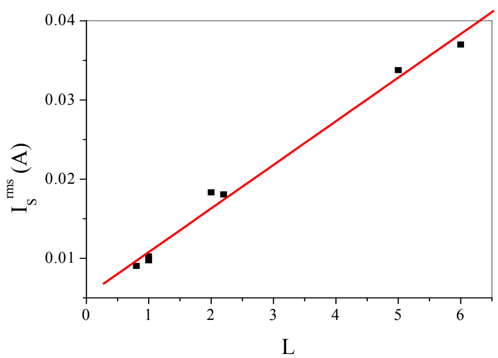

Figure 3.14 - The scaling factor versus the RMS of ion saturation current

The statistical properties of the radial coherence of fluctuations and transport have been computed from the maximum cross correlation of Γ_{ExB} and I_s signals radially separated 0.5 cm, using a 50 µs time window. The probability density distribution of the radial coherence of ExB transport shows tails (Figure 3.15) (i.e. sporadic events with high radial coherence). PDF´s of the radial coherence of fluctuations are more gaussian than those corresponding to the ExB turbulent flux. Although on average the radial coherence of turbulent transport is in the range of 0.5 – 1 cm, in agreement with previous findings, there are sporadic transport events showing large radial coherence. These results show the importance of the spectral characterization of both the radial scales of transport and fluctuations to improve our understanding of the physics underlying transport processes in fusion plasmas.

3.3.3.7. Velocity fluctuations and transport in the JET boundary region

A new approach for the measurement of turbulent fluxes and time dependent ExB sheared flows have been investigated in the JET plasma boundary region. It is based in the measurement of fluctuations in the phase velocity of fluctuations. Fluctuations in the radial ($\tilde{v}_r^{phase}$) and poloidal ($\tilde{v}_\theta^{phase}$) phase velocity have been computed from floating potential and ion saturation current signals using Langmuir probe arrays.

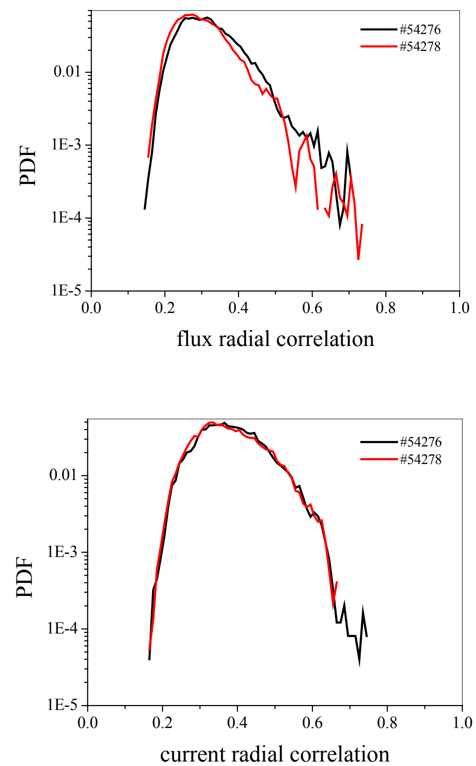

Figure 3.15 - PDF's of the radial coherence of ExB transport and ion saturation current fluctuations.

The radial velocity $\tilde{v}_r^{phase}$ is given by $\Delta r/\Delta t$, being ΔT the time delay between two ion saturation current (I_s) signals radially separated $\Delta r = 0.5$ cm. The time delay was computed using 200 µs time window realizations. The ExB turbulent flux was measured using two different approaches: a) from the correlation between density and poloidal electric field fluctuations using the expression

$$\Gamma_{E\times B} = < \tilde{n}\tilde{E}_\theta > / B \tag{3.4}$$

where $\tilde{E}_\theta$ is the fluctuating poloidal electric filed and ñ is the fluctuating density obtained from the ion saturation current, and b) from the correlation between density fluctuations and fluctuations in the radial phase velocity of fluctuations ($\tilde{v}_r^{phase}$) using the expression

$$\Gamma_{phase} = < \tilde{n}\tilde{v}_r^{phase} > \qquad (3.5)$$

Figure 3.16 show the time evolution of the turbulent flux deduced from expressions (3.4) and (3.5) in the plasma boundary region of JET ohmic plasmas (B = 1 T, Ip = 1 MA). Figure 3.17 shows the probability distribution function of the time resolved radial turbulent flux (Γ_{ExB} and Γ_{phase}). There is a significant similarity in the statistical properties of both turbulent fluxes. This agreement is particularly remarkable for the outward turbulent flux. The average turbulent fluxes, Γ_{ExB} and Γ_{phase}, are in agreement within a factor of four. This finding has been also observed using different time window realization (100 – 200 μs) for the computation of fluctuations in the radial phase velocity.

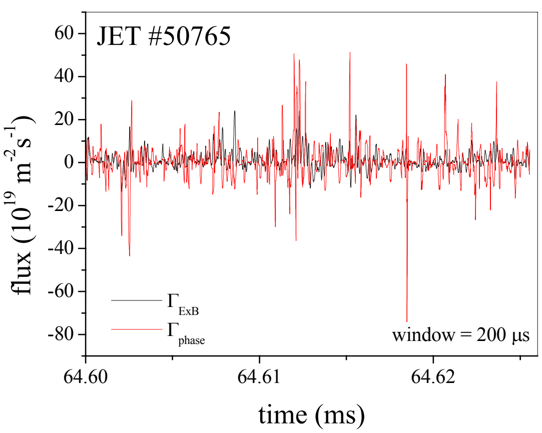

Figure 3.16 - Comparison between turbulent flux calculated within the electrostatic approximation and with the radial phase velocity of fluctuations

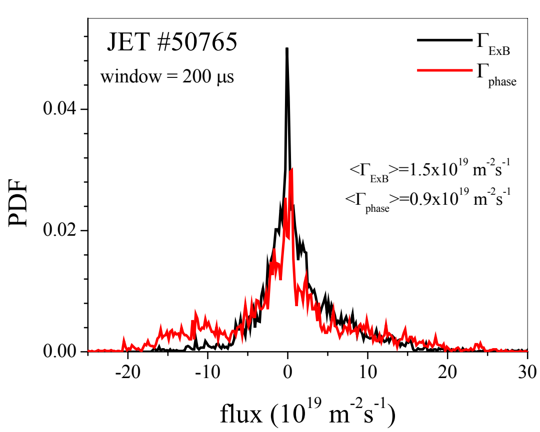

Figure 3.17 - Comparison of the Power Density Function of turbulent flux calculated within the two approaches

These results suggest that the measurement of ExB turbulent transport in the plasma core region can be achieved from measurements of density at different radial locations. Microwave Reflectrometry or Beam Emission Spectroscopy (BES) diagnostics can provide those measurements.

3.4. MICROWAVE REFLECTOMETRY

3.4.1. Introduction

The activities in this research area have been focused in the following topics:

- Calibration and operation of the kG3 O-mode reflectometer;
- Microwave propagation modelling and studies.

3.4.2. Calibration and operation of kG3 O-mode reflectometer

The main goal of this work was to show the ability of the KG3 reflectometer to produce good results for the estimation of the radial correlation lengths in the edge of the plasma, using its fixed frequency channels. Shot #53423 was used since it has a strong mode which appears to be a (3,2) tearing mode (and no ELMs in the interval studied), which in principle should allow the existence of large coherence lengths (~cm) within the plasma.

The localization of the reflectometer cut-off density layers was achieved using the density profile from the KE9 divertor LIDAR (Figure 3.18).

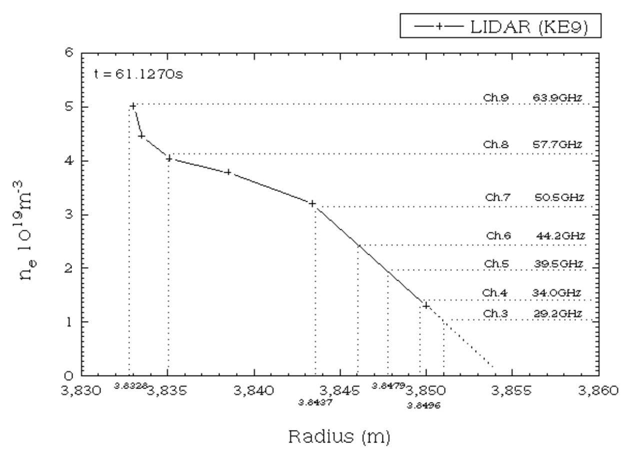

Figure 3.18 – Density profile from KE9 divertor LIDAR with the reflecting density layers for KG3 reflectometer indicated.

Figure 3.19 shows the temporal evolution of the power spectra of the signals corresponding to channels 3, 6 and 9 of the reflectometer KG3. Channels 3 and 6 present a mode during the whole interval, with a frequency of the order of 50 kHz. Channel 9 shows a similar feature, but only after t~61.53 s.

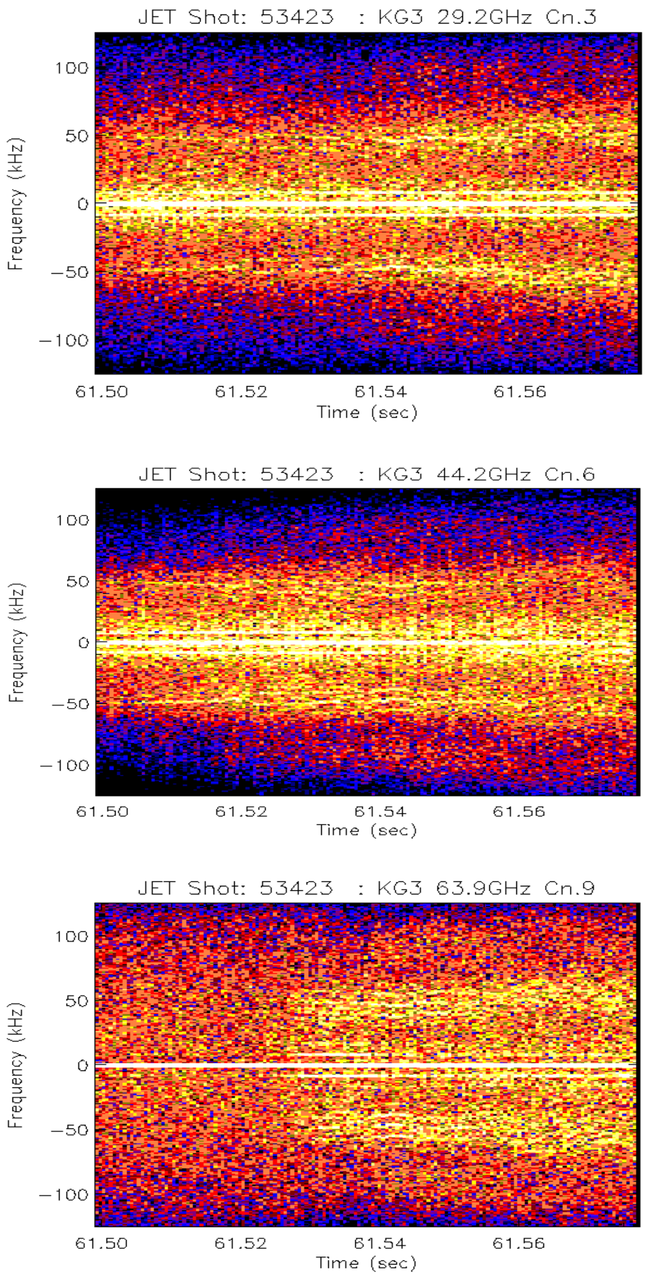

Figure 3.19 – Power spectra of channels with a 256 points (corresponding to 0.001024s) sliding window: (a) 3 → 29.2 GHz; (b) 6 → 44.2 GHz and (c) 9 → 63.9 GHz

The radial coherence lengths have been estimated by a first calculation of the coherence between one signal and the others (as in the example of Figure 3.20). Figures 3.21 and 3.22 are obtained by plotting the cross channel coherence against their layer separation[9]. From them we extract directly the radial coherence length which is the distance correspondent to a decrease of the coherence to the value of 1/e ≈ 0.37. We use only channels from 3 to 9 (and not channels 1, 2 and 10) as our ability to locate reflecting layers is limited by the density profile data available.

From Figure 3.20 it is clear that the cross coherence is evolving and two different temporal regions can be identified: from 61.50 s to 61.54 s and from 61.54 s to 61.58 s. The radial coherence plots of Figure 3.21 are obtained from the mean values of the cross coherence over the first temporal interval mentioned, while plots of Figure 3.22 correspond to the second one.

For the first temporal interval (from 61.50 s to 61.54 s), we see a good coherence between channel 3 and the others (Figure 3.21) – only the "homodyne" signals coherences are shown – leading to an estimate of radial coherence length of the order of several cm's, when going from the exterior to the interior. On the other hand, when going in the opposite direction, we found much less coherence between channel 9 and the others (Figure 3.22). This suggests that the coherent modes present in the signals are localized on a more external region of the plasma, and the loose strength when going further in the plasma. The hypothesis that the high coherence lengths observed are due to cross talk between the channels is overruled by the fact that in other discharges we find much smaller coherency, as the results of the previous section are an example. For the second temporal interval (from 61.54 to 61.58), we also get a good coherence when comparing channel 3 with the others (going from the outside to the inside of the plasma – Figure 3.22b). The coherence is particularly high for the "homodyne" (shown) signals and, as before, points towards a coherence length of several cm's. The more evident difference, compared to the previous time interval, comes when we calculate the coherency between channel 9 and the outer ones. Now the coherences are much higher than before, which corroborated by the power spectrum in Figure 3.19c), where we can see the mode appearing on channel 9 only after ~61.53 s.

[9] From the spatial separation of the reflecting layers, obtained from Figure 3.18.

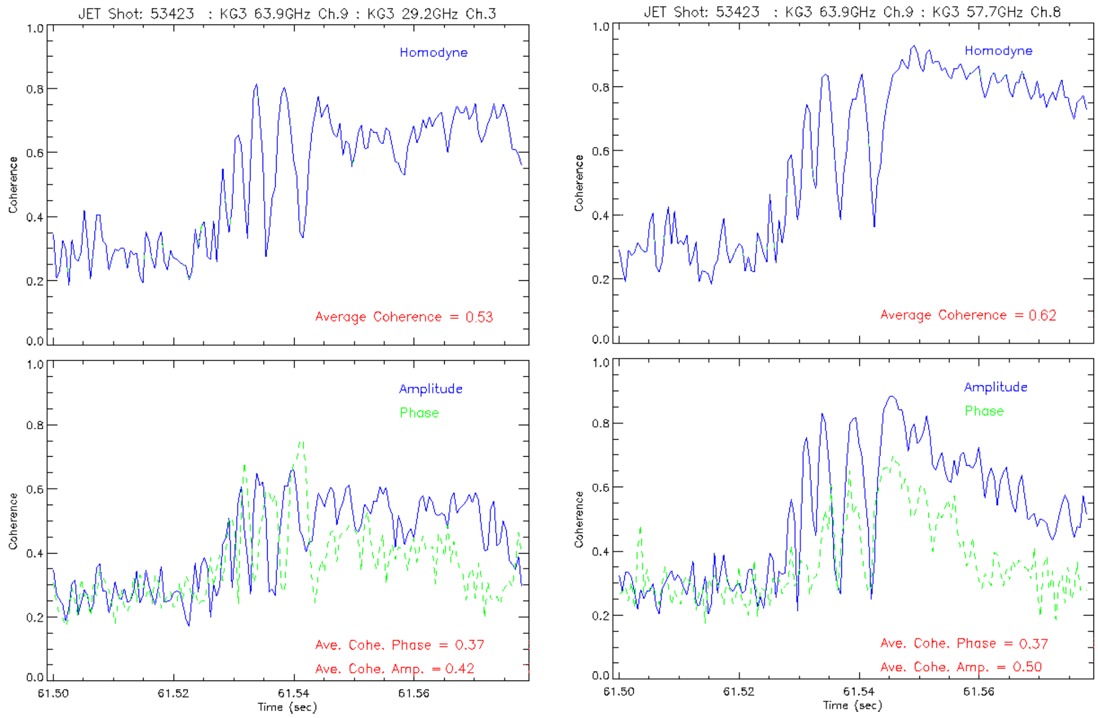

Figure 3.20 – Coherence between: (a) channel 9 and 8; and (b) channel 9 and 3. For each one of these, the top plot (1) uses "homodyne signals" and the bottom one (2) uses "amplitude and phase signals"

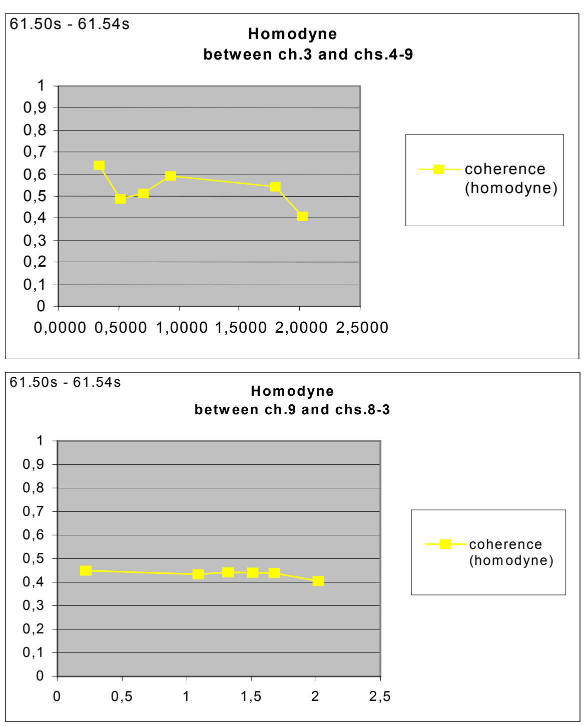

Figure 3.21 – Radial coherence (cm's) relative to (a) channel 3 → 29.2 GHz and (b) channel 9 → 63.9 GHz for the interval 61.50 s to 61.54 s from: (a) "homodyne signals"

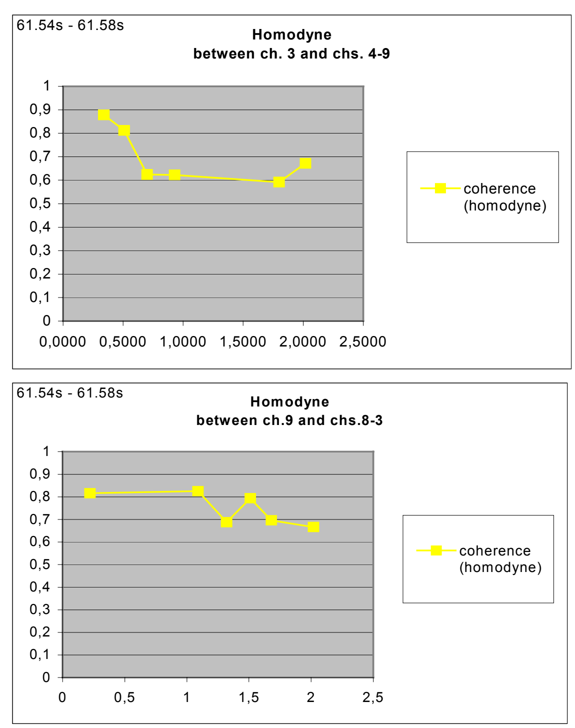

Figure 3.22 – Radial coherence (cm's) relative to (a) channel 3 → 29.2 GHz and (b) channel 9 → 63.9 GHz for the interval 61.54 s to 61.58 s from "homodyne signals"

The analysis presented, following the calibration procedures performed, fulfilled the goal of illustrating the ability of the reflectometer KG3 to perform correlation studies on the edge region of the plasma. In terms of the physical phenomena involved, this study is far from being complete and should continue, namely through the more precise characterization on the mode present on this particular discharge. Also important should be the localization of the cutoff layer with respect to the q profile, needed if one wants to investigation the transport properties of the discharge. Finally, it is worth noting that in this and on further correlation studies, it is fundamental to check the density profiles available (KE3 and KE9) in order to decide which one is the more reliable for the discharges under study.

The future work should involve making more calibration acquisitions and similar studies for other shots, making also a consistent comparison with other diagnostic (namely the magnetics) to benchmark and further develop the conclusions. The studies should also be complemented by the information given the KG8 correlation reflectometer, which is able to look further inside the plasma.

3.4.3. Microwave propagation modelling and studies

In the frame of the Task Force D, the work developed was mainly focussed on the modelling of reflectometry measurements with JET reflectometers. The two reflectometers KG3 and KG8b installed on JET allow a large variety of measurements (O or X mode, radial, poloidal or toroidal correlations) which are useful to study the turbulence behaviour during all kinds of confinement regimes (L mode, H mode, ITBs, …). To help at this interpretation of these measurements, the main part of the work has been to develop a code simulating the KG3 reflectometer.

The code resolves the following 2D O-mode full-wave equation obtained from Maxwell equations under cold plasma approximation:

$$\left[\frac{\partial^2}{\partial t^2} - c^2\frac{\partial^2}{\partial x^2} - c^2\frac{\partial^2}{\partial y^2} + \omega_{pe}^2(x,y,t)\right] E(x,y,t) = 0 \qquad (3.6)$$

This code has been adapted to the KG3 reflectometer characteristics (two antenna configuration, position and size of the wave-guides). Density profiles measured by LIDAR and KE9D have been input in the code using the following procedure: (i) first an interpolation method has been used to get a smooth density profile from LIDAR and KE9D radar data; (ii) 2D density profiles have been then deduced from the poloidal symmetry given by FLUSH and FLUPN subroutines.

Examples of electric field contour plot obtained from the 2D code were obtained using probing waves reflected in the flat region of the ITB pedestal, thus explaining the observed scattering of the electric field. These simulations have been computed for frozen density profiles so that the resulting electric field reaches a stationary regime after a certain time. Depending on the type of density profile, the time required to reach this stationary regime can be longer, as is the case of a flat density profile with a cavity behind the cut-off region, due to the wave trapping phenomena occurring in the cavity.

The work carried showed the potentialities of full-wave simulations to help at the interpretation of reflectometry experiments. A stronger interaction with experimental results is now planned that should allow in particular to get a better understanding of turbulence behaviour during the various scenarios observed on JET (H mode, ITBs, …). The development of a X-mode 2D full-wave code could be also envisaged that would allow comparisons with KG8b correlation reflectometer.

3.5. JET ENHANCED PERFORMANCE PROJECT

3.5.1. Introduction

IST/CFN has been involved in the following JET Enhanced Performance (JET-EP) Projects (Table 3.3):

- Study of turbulence by microwave reflectometry;
- Microwave interferometer;
- Mw access;
- Reflectometry system for the ICRF antenna

3.5.2. Study of turbulence by microwave reflectometry

3.5.2.1. Introduction

This Project involves the development of two channels of correlation reflectometers and the dedicated data acquisition system, aiming at studying electrostatic turbulence at the plasma core with good spatial and temporal resolutions, namely in the region where internal transport barriers are formed.

Project	Contract	Beginning	End
Study of turbulence by microwave reflectometry	FU05-CT-2000-00241	22/12/2000	31/12/2002
	FU05-CT-2000-00242	22/12/2000	31/12/2002
Microwave interferometer	FU05-CT-2000-00244	08/11/2001	31/12/2002
µW access	FU05-CT-2000-00303	08/11/2001	30/01/2003

Table 3.3 – Contracts of IST/CFN concerning JET-EP Projects

The IST/CFN participation in this Project has involved:

- The responsibility of the project (Dr. Luis Cupido;
- The development, testing and installation at JET of the reflectometers and the dedicated data acquisition system.

The following main activities were performed in 2001:

- Finalisation of the conceptual designs of the reflectometers and their data acquisition system;
- Realisation of the procurement procedures;
- Development of microwave circuits as well as data acquisition hardware and software;
- Commissioning and testing of the microwave reflectometers and data acquisition system in the IST/CFN Laboratories;
- Delivery of the equipment to JET.

3.5.2.2. Microwave reflectometer

The correlation reflectometers developed by CFN operate at the V band and consist of a dual receiver phase and amplitude reflectometer (Figures 3.23 and 3.24). It employs an operating scheme tested a previously at JET on KG3 (equipment constructed by CFN delivered to JET during 1999).

This instrument has two millimetre wave sources one that is fixed in frequency and one that can be tunned within 2 GHz. The oscillators are differentially locked and the frequency control is done using the same frequency control technology used for the ASDEXupgrade fluctuations monitor system. In order to tune within the 2GHz bandwidth in less than 2ms the frequency control for this instrument can operate in synchronous mode having each frequency change triggered by an external pulse rather then asynchronous RS232 control. To fully exploit the frequency agility of this instrument a special trigger was generated synchronously with the data acquisition (Figure 3.24).

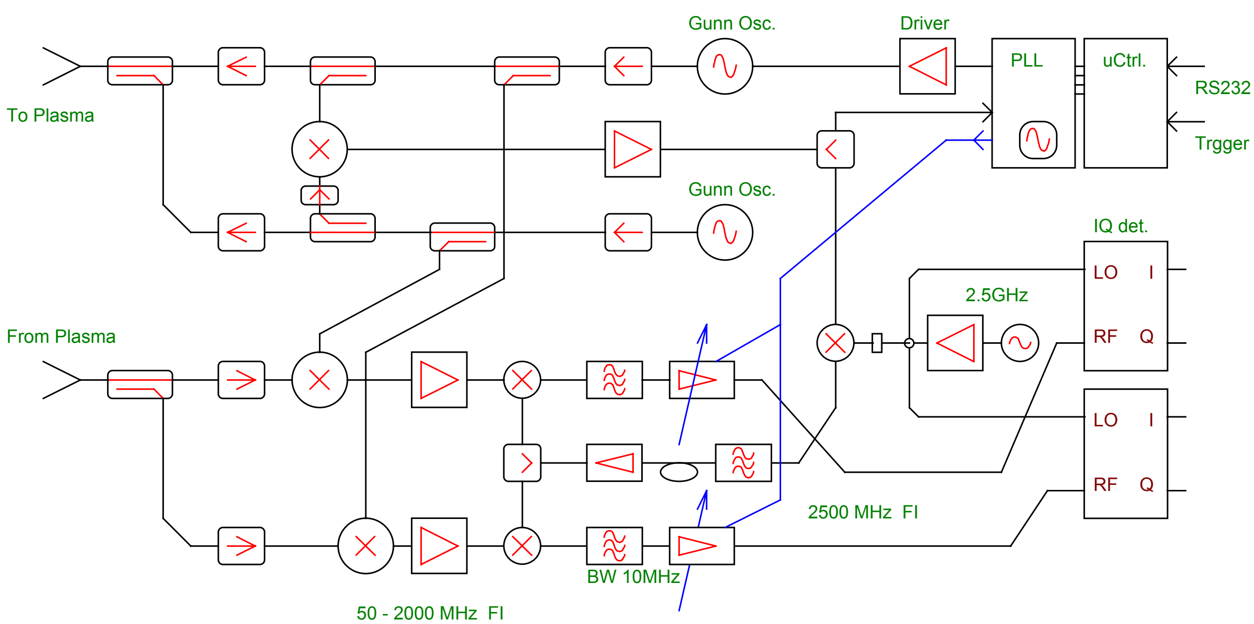

Figure 3.23 - Schematic configuration of the correlation reflectometer to study turbulence at the JET plasma core

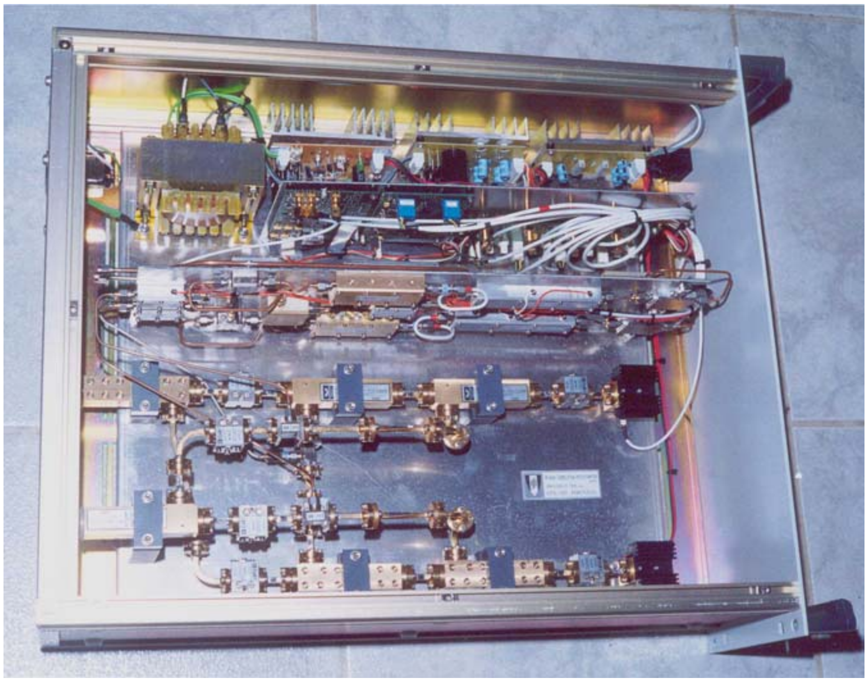

Figure 3.24 – View of the experimental device

3.5.2.3. Data acquisition system

The dedicated VME data acquisition system has been developed aiming at to have large memory and high data transfer rate. It is composed by (Figure 3.25):

- One CPU module, with a Pentium III processor running RTLinux, 256 MB RAM, four RS232 ports, one 10/100 Mbits/s Ethernet channel and one 4 GB disk;
- Two on-site developed intelligent transient recorder modules (TRMs), with one Digital Signal Processor (DSP) TMS320C31 running at 80 MHz, 8 input channels with 16 bit resolution at sampling rates up to 250 kSPS per module, and 64 kWords of memory;
- Two on-site developed fast transient recorder modules, each one having 8 input channels, with 12 bit resolution, 1.5 Msample memory and sampling rate up to 3 MSPS;
- Software for the interface with the JET network and for the system and diagnostic operation.

The intelligent transient recorder modules (Figure 3.26) have the following main functions:

- to provide the system acquisition clock frequency up to 3 MHz, and 1 ms time resolution to control the measurement series length;

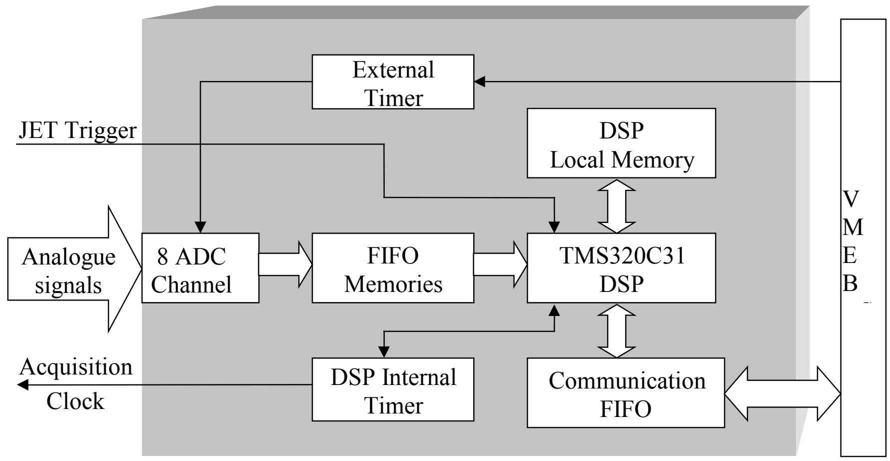

Figure 3.26 – Block diagram of the intelligent transient recorder module

- to acquire 16 channels at a slow rate for real time plasma monitoring in order to detect the turbulence;
- to run a digital signal processing algorithm over the acquired data to avoid the use of the old KG8B root mean square (RMS) analogue circuits.

Figure 3.27 depicts a block diagram of one of the eight channels of the fast transient recorder modules (TRM). Each acquisition channel can store 1.5 Msamples of 12 bits, required to acquire a large quantity of data with no dead time (see section 4). To control the data flow from ADC (LTC1412) to the channel memory and to VME bus, an address generator was implemented in a Programmable Logic Device (PLD), along with all the logic control.

The purpose of these modules is to digitise and store the incoming analogue signals from reflectometers at a 2MSPS per channel rate.

The two fast TRMs can achieve an overall acquisition rate up to 96 Mbytes/s, which cannot be sustained when data is transferred from the acquisition boards to some other system resource due to the limitations of the VME bus performance. Optimal VME interfaces are required to minimise dead time between acquisitions. For this reason the transient recorder slave modules support Block Transfer Accesses and the master CPU module uses an industry leading VME controller.

The software controlling this device allows the user to configure the acquisition periods and thus compromising the number of measurement series, its duration and the available memory.

The communication between the JET central control and data acquisition systems and this dedicated data acquisition system will be made using a 100 Mbits/s Ethernet channel, to receive commands and send the acquired data. This choice was made based on the standardisation, performance and low cost of this technology.

The data acquired during one JET discharge is stored in the JET database after all diagnostic activities are over, at the end of the JET discharge. The diagnostic configuration will also be obtained from the JET computers through the network before the beginning of the discharge.

3.5.3. Microwave interferometer

This Project consists in the upgrade of the existing microwave diagnostics in the divertor region.

The following main activities were carried out:

- Assessment of the existing transmission line and antennas;
- Beginning of a new design for the antenna and waveguide routing, aiming at to improve the performance if these diagnostics, allowing a better understanding in the divertor physics;
- Beginning of the developing of numerical codes that provide the electromagnetic field pattern and the radiation diagrams of the launching and receiving antennas;
- Beginning of the development of a ray tracing code to study the propagation conditions of the launched waves in the plasma.

3.5.4. Mw - access

This Project aims a new access for the microwave diagnostics (ECE and reflectometry), being the Association EURATOM/IST the leading Association (Dr. Luis Cupido is the Project Leader).

The following main activities were performed:

- Participation in a meeting in Culham;
- Beginning of the conceptual study of the project;
- Elaboration of the preliminary specifications of the project.

3.5.5. Reflectometry systems for the ICRF antenna

This project consists on the design of a two-channel X-mode reflectometer to be included in the future ICRH antenna.

The following main activities were carried out:

- Assessment of the possibilities for the transmission line routing and antenna installation;
- Selection of the frequency bands.

3.6. MANAGEMENT

3.6.1. Introduction

IST/CFN has collaborated on the management of the use of the JET Facilities by the EFDA Associates in the following manner:

- Prof. Fernando Serra is member of the EFDA Sub-Committee for JET (JSC);
- Dr. Duarte Borba belongs to the staff of the Close Support Unit (CSU) to the EFDA Associate Leader for JET, since April 1st 2000;
- Profª. Maria Emília Manso was member of the Ad-Hoc Groups for Phase II evaluation of the JET Enhancement Project;
- Prof. Fernando Serra is member of the Ad-Hoc Group for the Assessment of the diagnostics requirements for the JET Enhanced Performance Project;
- Prof. H. Fernandes and Mr. P. Varela belong to the Remote Participation Users Group.

3.6.2. Responsibilities and main activities

The main activities carried out in 2001 were:

- Prof. F. Serra attended six meetings of the EFDA JET Sub-Committee;
- Mr. Duarte Borba has been seconded to the EFDA-Close Support Unit, Culham. During this period he is part of the Programme Department (Head: Dr. M. Watkins) and reports to the Associate Leader for JET (Dr. J. Pamela). As Responsible officer for Task Force M, the main duties are to assist in establishing the scientific contends, necessary staffing and the necessary competencies for the JET scientific Workprogramme and assist in the preparation of S/T (Scientific/Technical) Orders and Notifications. In addition, as responsible officer for codes and data, the main duties are to establish links between Taskforces and the JOC regarding the data analysis and validation;
- Profª. Maria Emília Manso participated on one meeting of the Ad-Hoc Group on JET-EP;
- Prof. F. Serra attended three meetings of the Ad-Hoc group for diagnostics enhancements;
- Prof. H. Fernandes and Mr. P. Varela attended one meeting each of the Remote Participation Users Group.